Supplementary information

Experimental

Sample preparation. A simple approach based on gas-solid reactions was used to modify the sulfide electrolyte. 500 mg of Li_6PS_5Cl or $Li_7P_3S_{11}$ powder (Guilin Electrical Equipment Scientific Research Institute Co. Ltd.) was sealed in a bottle in an Ar-filled glovebox. Then, 99.999% O_2 or 99.9% CO_2 flowed through the bottle at the rate of 100 ml/min as illustrated in Fig. S2. After being exposed for different times, the gas-treated electrolyte samples were harvested and stored in the Ar-filled glovebox for subsequent utilization. Li_6PS_5Cl with a smaller particle size was obtained via ball milling the original sample at 400rpm for 12h in Ar or CO_2 atmosphere. Li_2CO_3-coated $LiCoO_2$ was synthesized by annealing the bare $LiCoO_2$ (Aladdin) at 600 °C in the CO_2 atmosphere for 2h.

Conductivity measurements. The ionic conductivity was measured by EIS. Typically, ~80 mg of the electrolyte powder was pressed into a pellet using a 10 mm PEEK die under a pressure of 370 MPa. EIS measurements were conducted from 1 MHz – 1 Hz with an amplitude of 50 mV. The thickness of the pellet was around 0.5 - 0.7 mm. For the moisture toleration tests, LPSC samples were first exposed to the ambient air with a relative humidity of 17% for 1 hour before EIS measurements. The electronic conductivity was obtained with direct current (DC) polarization by applying a 0.5 V bias potential for 10 h with titanium rods as blocking electrodes. All the EIS tests and DC polarization tests were performed at room temperature using an SP-200 system (Bio-logic) in an Ar-filled glovebox.

Electrochemical measurements. ASSBs were assembled in an Ar-filled glovebox without special instruction. Typically, in the case of half cells, ~80 mg of electrolyte powder was first placed into a PEEK die (diameter of 10 mm) and pressed at 1 ton for 1 min. Then 8 ~ 10 mg of cathode composite (corresponding to an areal mass of 10.2-12.7 mg/cm^2) was spread onto this pellet. After that, a Li foil (Φ8mm, 1.25 mg) and an In foil (Φ10mm, 55.40 mg) were attached to the other side of the pellet and re-pressed at 1 ton for 5 min to form a sandwich-like structure. Then the cells were placed into a steel casing with a stack pressure of ~300 MPa. In the case of Si||SE||LCO full batteries, the Li-In alloy foil was replaced by anode composites (micro Si: SE = 7:3 in mass, N/P ratio of 1.2). For the cathode composite, $LiCoO_2$ powder was mixed in a 7:3 mass ratio with SE, and $LiNi_{0.815}Co_{0.15}Al_{0.035}O_2$ powders (MTI) were mixed with SE and VGCF (Canrd) in a mass ratio of 70:30:1. All materials were used as received without any treatment.

To imitate the practical manufacturing process, synthetic air was pumped into a CO_2-filled glovebox and thus different atmospheres with CO_2 concentration of 0.075 % and 45.8% was obtained. The dew point was controlled at around -25 °C ~ -30 °C. ASSBs using pristine LPSC were assembled inside this glovebox within 30 mins following the same fabrication procedures described above.

Galvanostatic cycling for all batteries was carried out in an Ar-filled glovebox at room temperature using a Neware battery test system (CT-4008T-5V10mA-164). The voltage range for Li-In||SE||LCO half cells was 2 V – 3.9 V and 1.9 V – 3.7 V for Li-In||SE||NCA half cells. And Si||SE||LCO full cells were cycled between 2.5 V and 4.35 V. Rate current densities were calculated based on the conventional reversible capacity of LCO (1C = 150 mA/g) and NCA (1C = 180 mA/g). After cycling for 300 or 1000 cycles of LCO half cells, EIS was conducted under a frequency of 1 Mhz – 10 mHz with an amplitude of 10 mV.

Materials characterization. After cycling, cells were disassembled in an Ar-filled glove box. The X-ray photoelectron spectra (XPS) characterization was implemented on a Thermo Fisher Scientific ESCALAB 250 Xi with monochromatic 150 W Al Kα radiation. All the samples were transferred from the glove box to the XPS chamber using a sealed vessel to avoid exposure to air. The TEM and EELS characterizations were conducted on the JEOL ARM200F. To minimize the damage from the electron beam, a liquid nitrogen cryo-EM holder (Fischione 2550) was employed. The elemental distribution was obtained by a Hitachi S-4800 scanning electron microscope (SEM) equipped with an EDX detector. The X-ray diffraction (XRD) patterns were collected using the Cu Kα radiation on a Bruker D8 Advance Diffractometer. Raman spectra were collected on Horiba LabRAM HR Evolution Raman spectrometer with 532 nm radiation. The TG-MS analysis was performed on an STA 449 F3 (NETZSCH) simultaneous thermal analyzer coupling with a QMS 403 (NETZSCH) mass spectrometer. Before CO_2 flowed (100 mL/min), Ar was purged for 1h to set the baseline. TOF-SIMS was conducted using a TOF.SIMS 5 system (IONTOF GmbH). And depth profiles were acquired using a Cs^+ sputtering ion beam (1 keV ion energy). Fourier transformed infrared spectra (FTIR) were recorded on a Bruker VERTEX 70 V spectrometer. The content of CO_2 was measured by a gas chromatography (GC) system (Shimadzu Nexis GC-2030) equipped with a barrier ionization discharge (BID) detector.

DFT calculations. The DFT calculations were performed with Vienna ab initio simulation package (VASP)[1] by using the generalized gradient approximation (GGA) and the exchange-correlation function from Perdew–Burke–Ernzerhof (PBE)[2]. The structural optimizations are finished with the energy/force convergence are 10^{-5} eV and 0.01 eV/Å with relaxing both the atom sites and the cell shape. The cutoff energy is 520 eV, and the k-mesh used to sample the Brillouin zone is in the density of one point per 0.05 $Å^{-3}$ including the Gamma point. The structures of Li_5PS_5Cl were generated from Li_6PS_5Cl with four Li removed by group theory[3] and the structure with minimum energy was selected. (Fig. S11) The CO and CO_2 molecular were calculated with one molecular in a 10 Å× 10 Å× 10 Å box. The pseudo-binary phase stabilities were calculated based on the energies obtained from the Materials Project database.

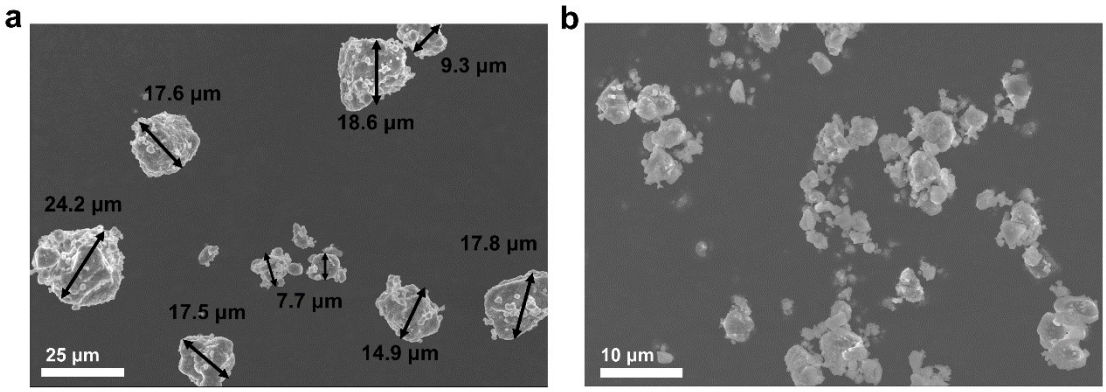

Fig. S1 SEM images showing the particle size distribution of the pristine LPSC (a) and the ball-milled LPSC (b) samples. The particle size of the original LPSC is ranging from 7 μm to 24 μm, which is reduced to around 400 nm~6 μm after ball milling.

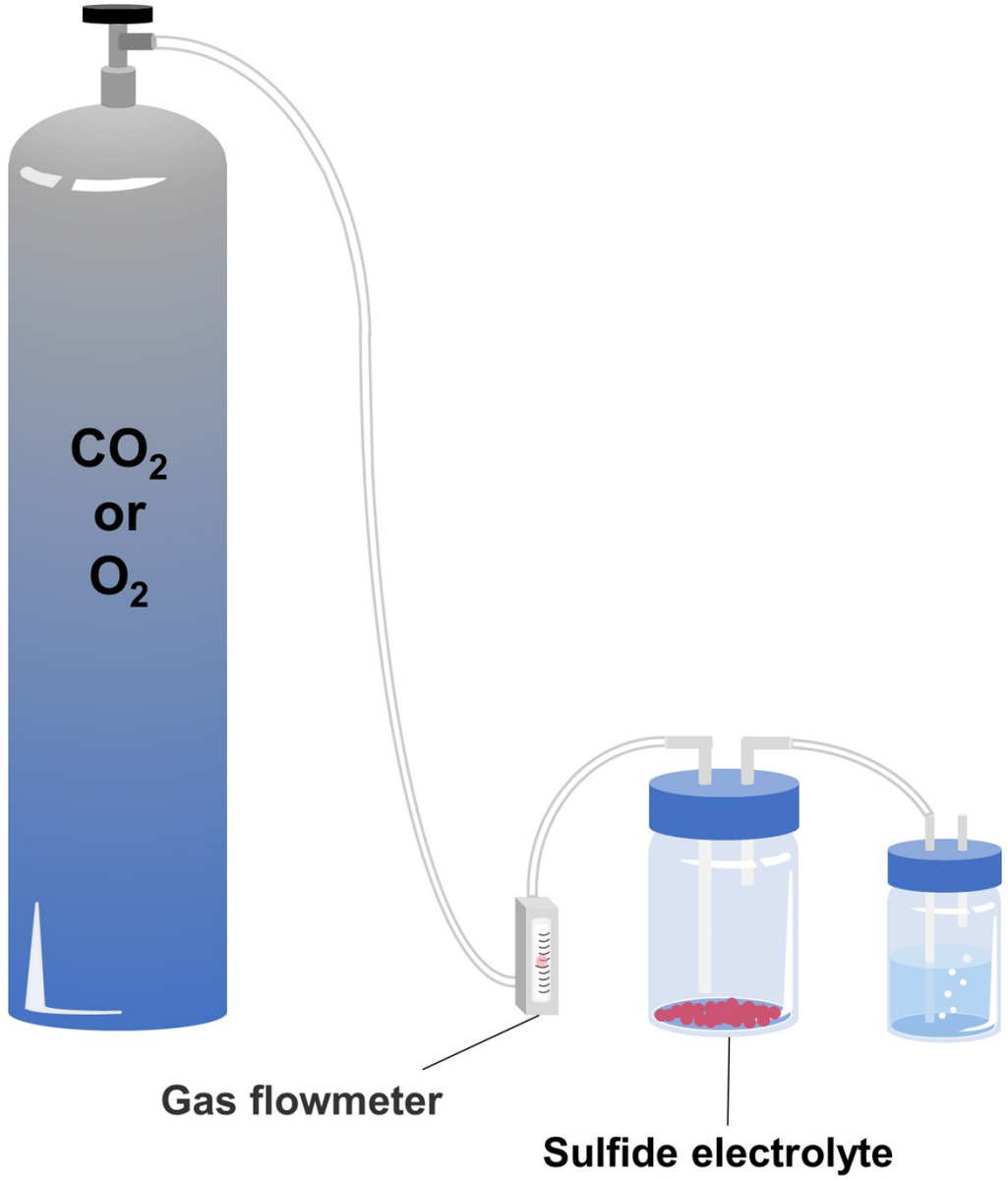

Fig. S2 Schematic illustration of the preparation process of gas-treated electrolyte.

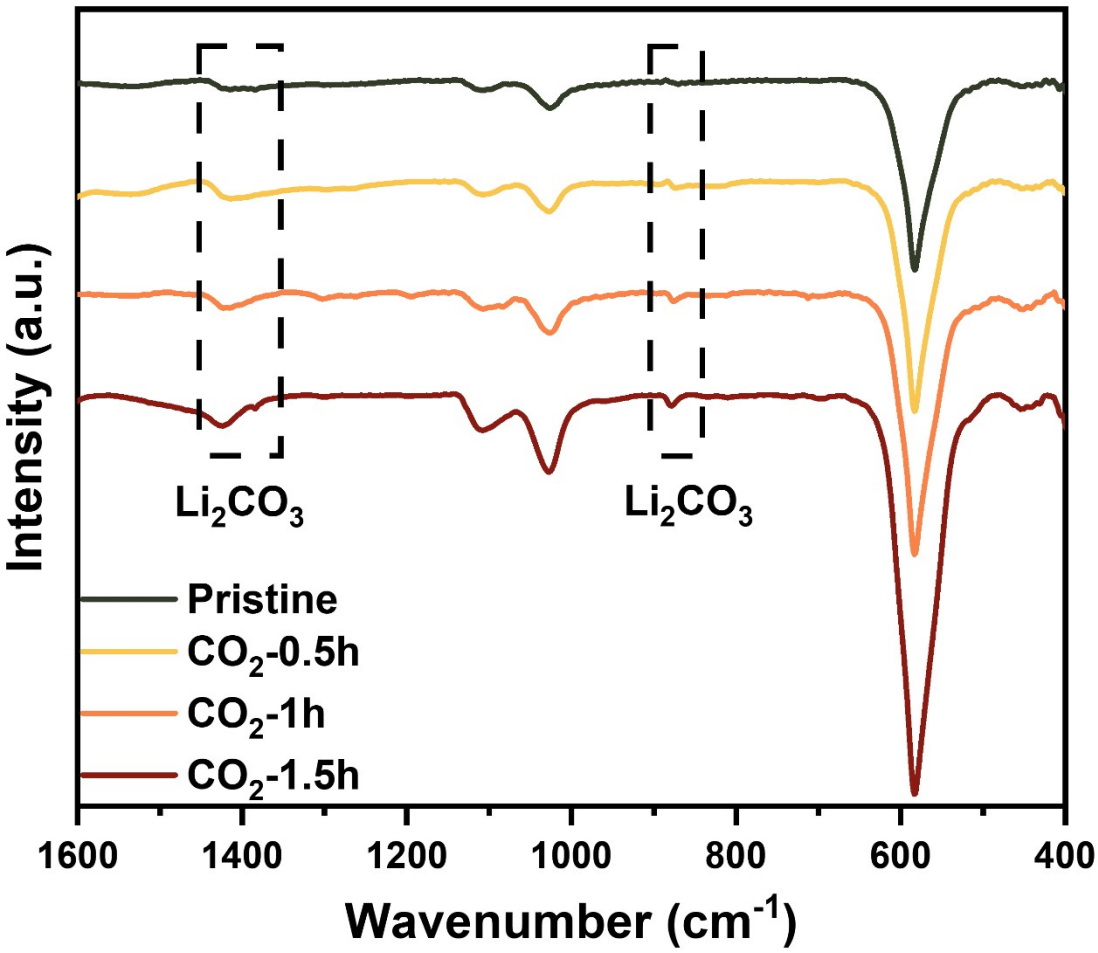

Fig. S3 FT-IR patterns of the pristine LPSC and CO_2-treated LPSC. The peaks at 1435 cm^{-1} and 879 cm^{-1} related to the typical vibration of Li_2CO_3.[4]

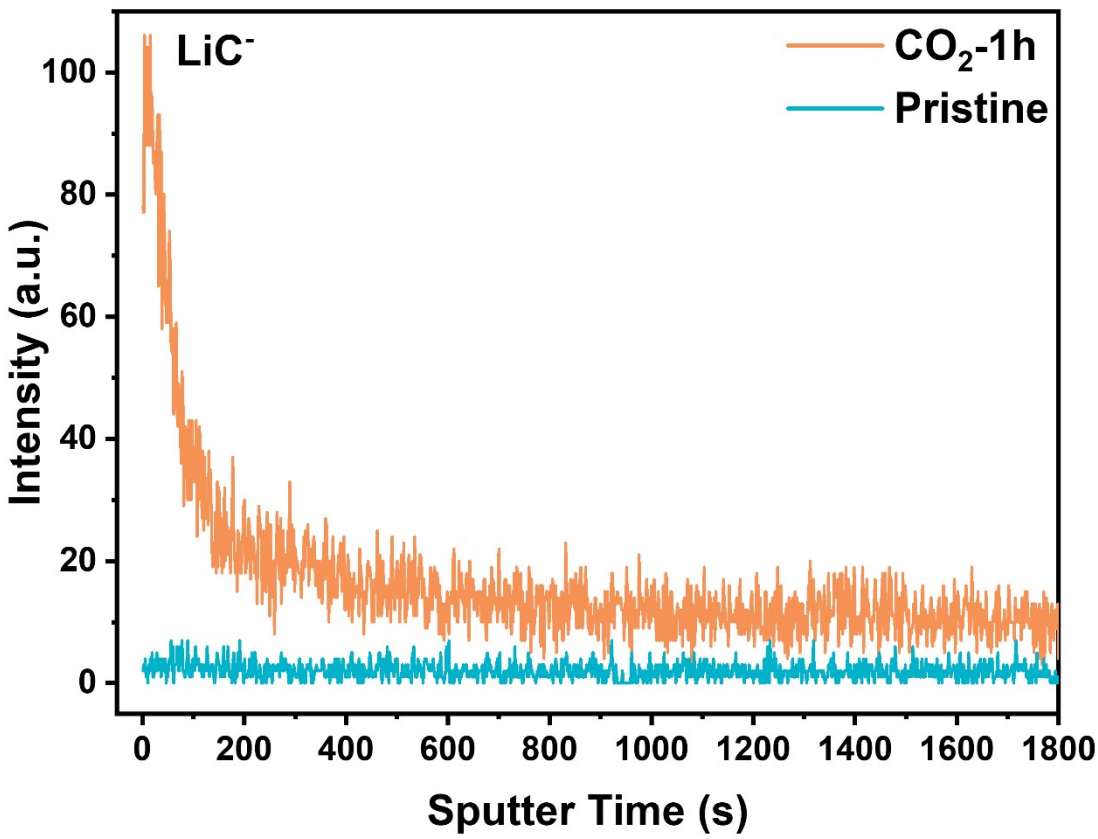

Fig. S4 TOF-SIMS results of LiC^- fragment for the pristine LPSC and CO_2-1h LPSC.

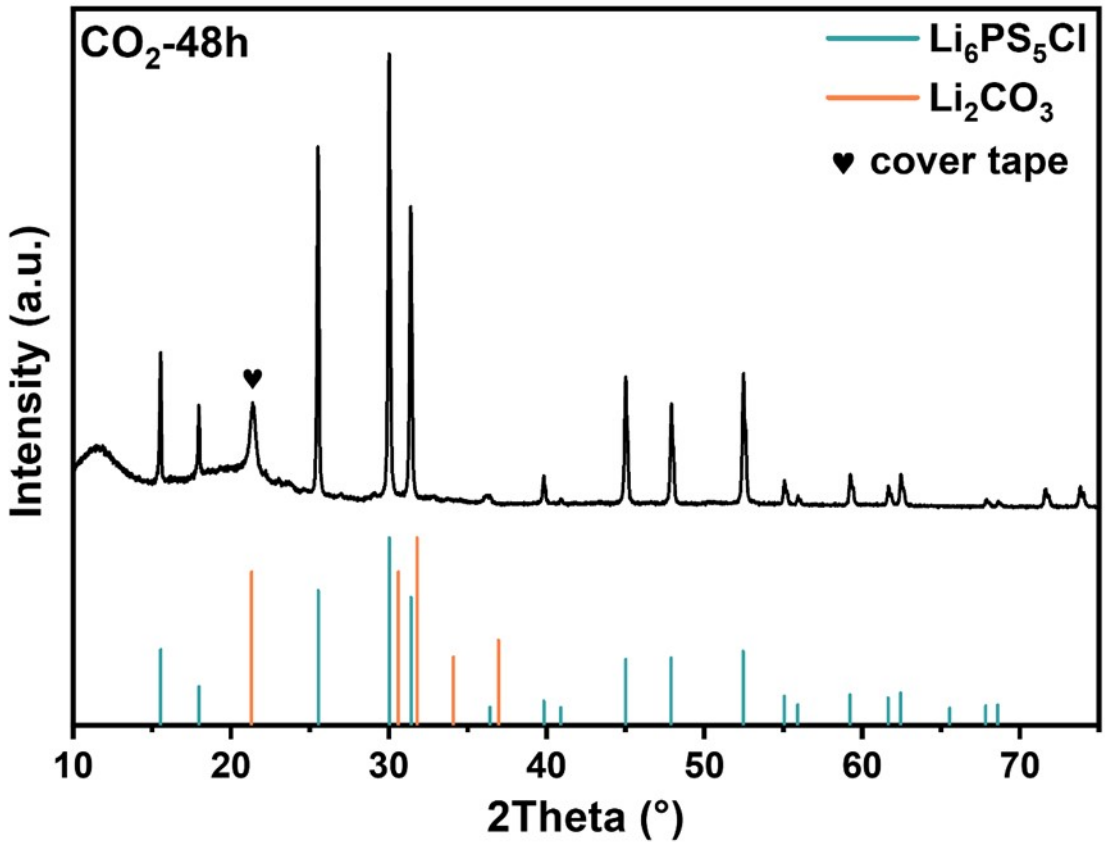

Fig. S5 XRD spectra of the CO_2-48h LPSC samples. None of the peaks belonging to Li_2CO_3 is observed.

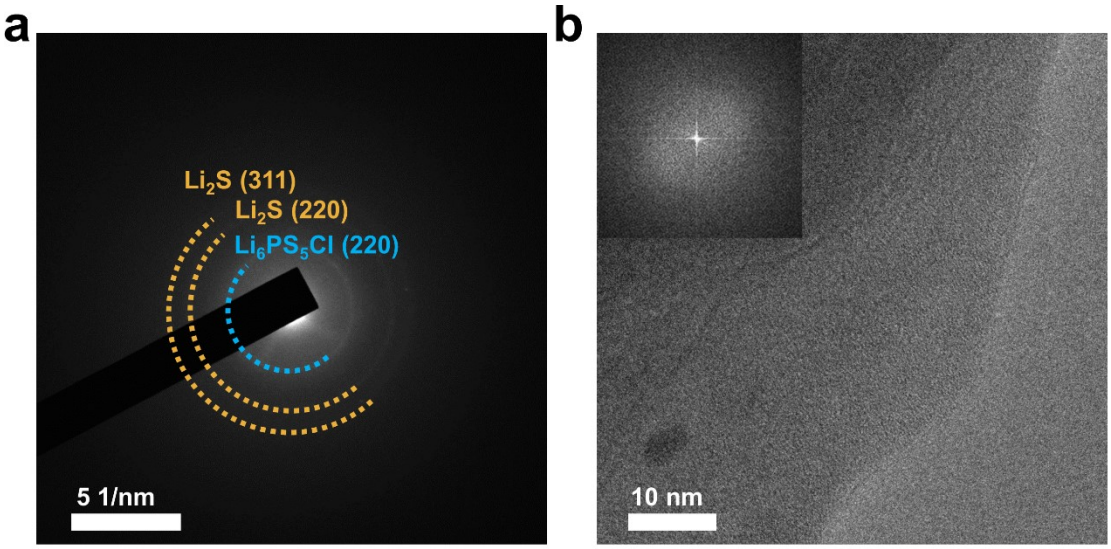

Fig. S6 Cryo-TEM image of CO_2-1h LPSC. (a) The selected area electron diffraction (SAED). (b) HR-TEM image, and the corresponding FFT image (inset). None of the diffraction patterns or lattice fringe belonging to Li_2CO_3 was observed in SAED or HR-TEM indicating that the as-formed Li_2CO_3 layer is amorphous. The presence of Li_2S in the diffraction pattern is due to the decomposition of LPSC under irradiation, which demonstrates the ultra-beam sensitivity of LPSC.

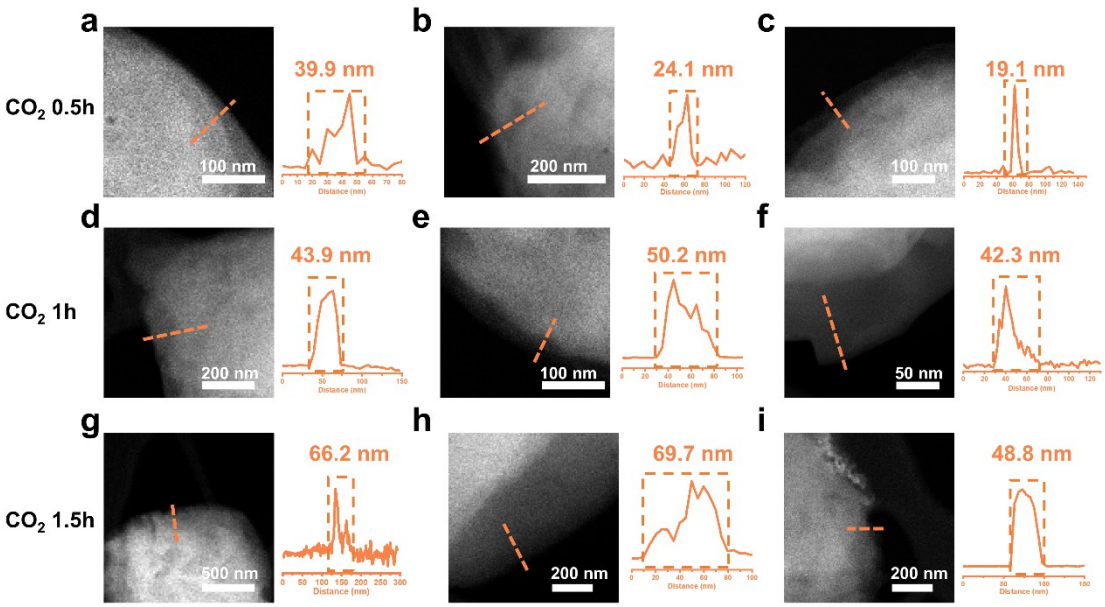

Fig. S7 Thickness of Li_2CO_3 layer in the CO_2-treated LPSC samples measured by the EELS line scan profile of Li_2CO_3 signal at 285 eV. (a-c) Three different particles of CO_2-0.5h LPSC. (d-e) Three different particles of CO_2-1h LPSC. (g-i) Three different particles of CO_2-1.5h LPSC. The Li_2CO_3 thickness is 19~40 nm, 42~50 nm, 49~70 nm for CO_2-0.5h, 1h, and 1.5h LPSC, respectively.

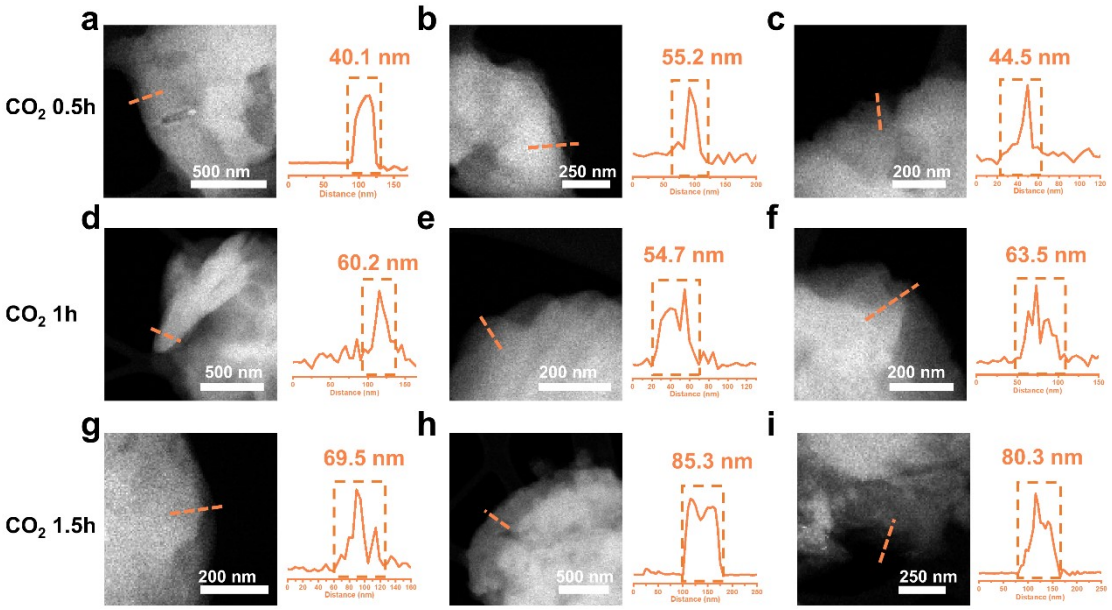

Fig. S8 Thickness of Li_2CO_3 layer in the CO_2-treated LPSC samples measured by the EELS line scan profile of Li_2CO_3 signal at 285 eV. (a-c) Three different particles of CO_2-0.5h LPSC. (d-e) Three different particles of CO_2-1h LPSC. (g-i) Three different particles of CO_2-1.5h LPSC. The Li_2CO_3 thickness is 40 nm~55 nm, 55 nm~64 nm, and 70 nm~85 nm for CO_2-0.5h, 1h, and 1.5h LPSC, respectively.

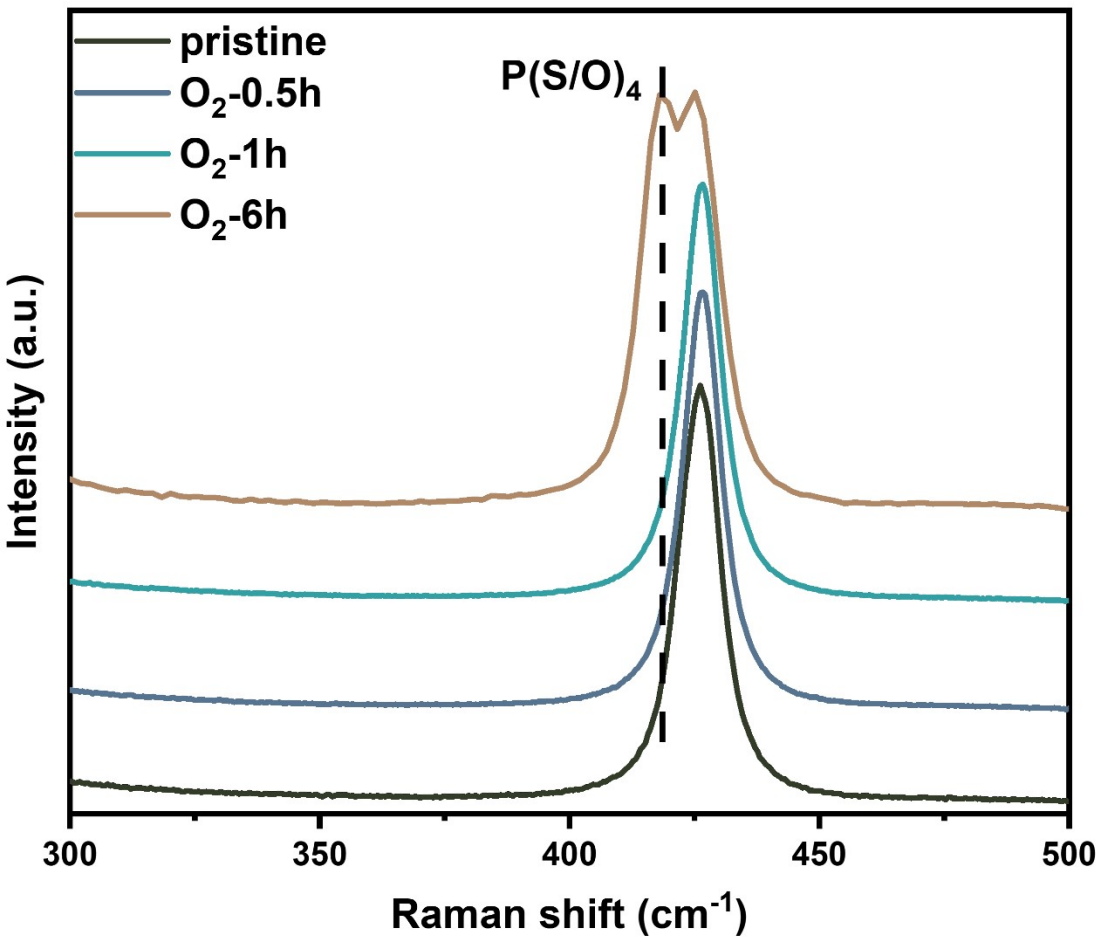

Fig. S9 Raman spectra of O_2-treated LPSC sample. The new peak appearing at 418 cm^{-1} implies the formation of oxysulfide.

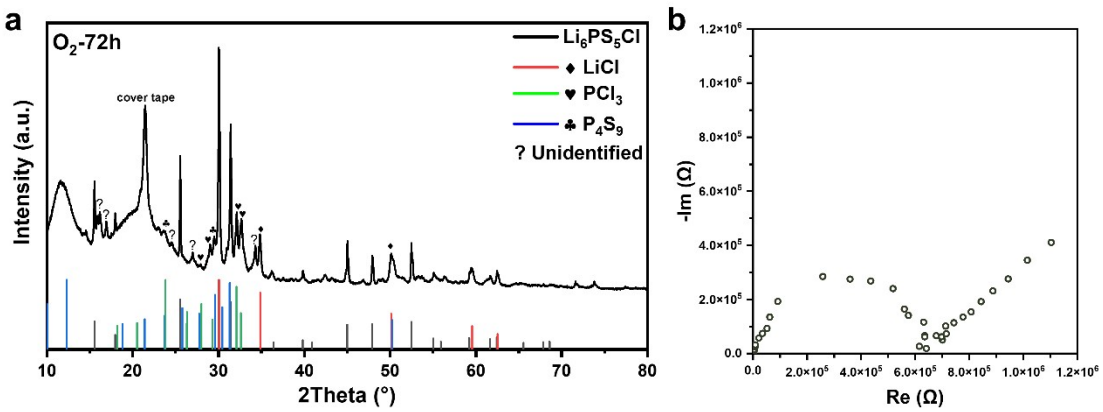

Fig. S10 Decomposition of the LPSC in O_2 for 72h. (a) XRD spectra of the O_2-72h LPSC sample. (b) Impedance of O_2-72h LPSC sample. Long-time exposure to O_2 will induce LPSC decomposition.

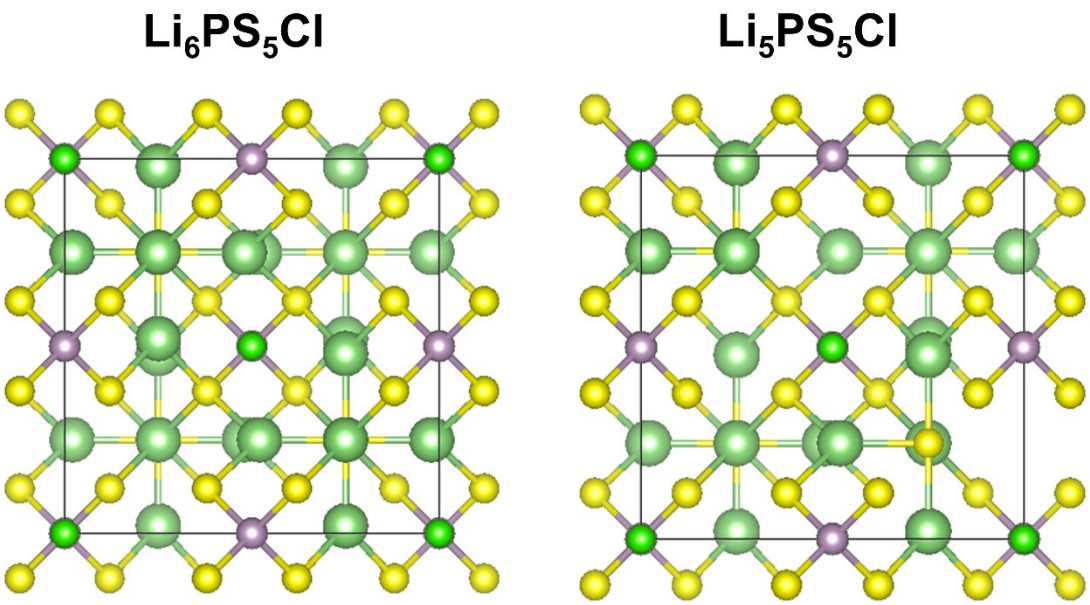

Fig. S11 Structure of Li_6PS_5Cl and Li_5PS_5Cl screened by group theory.

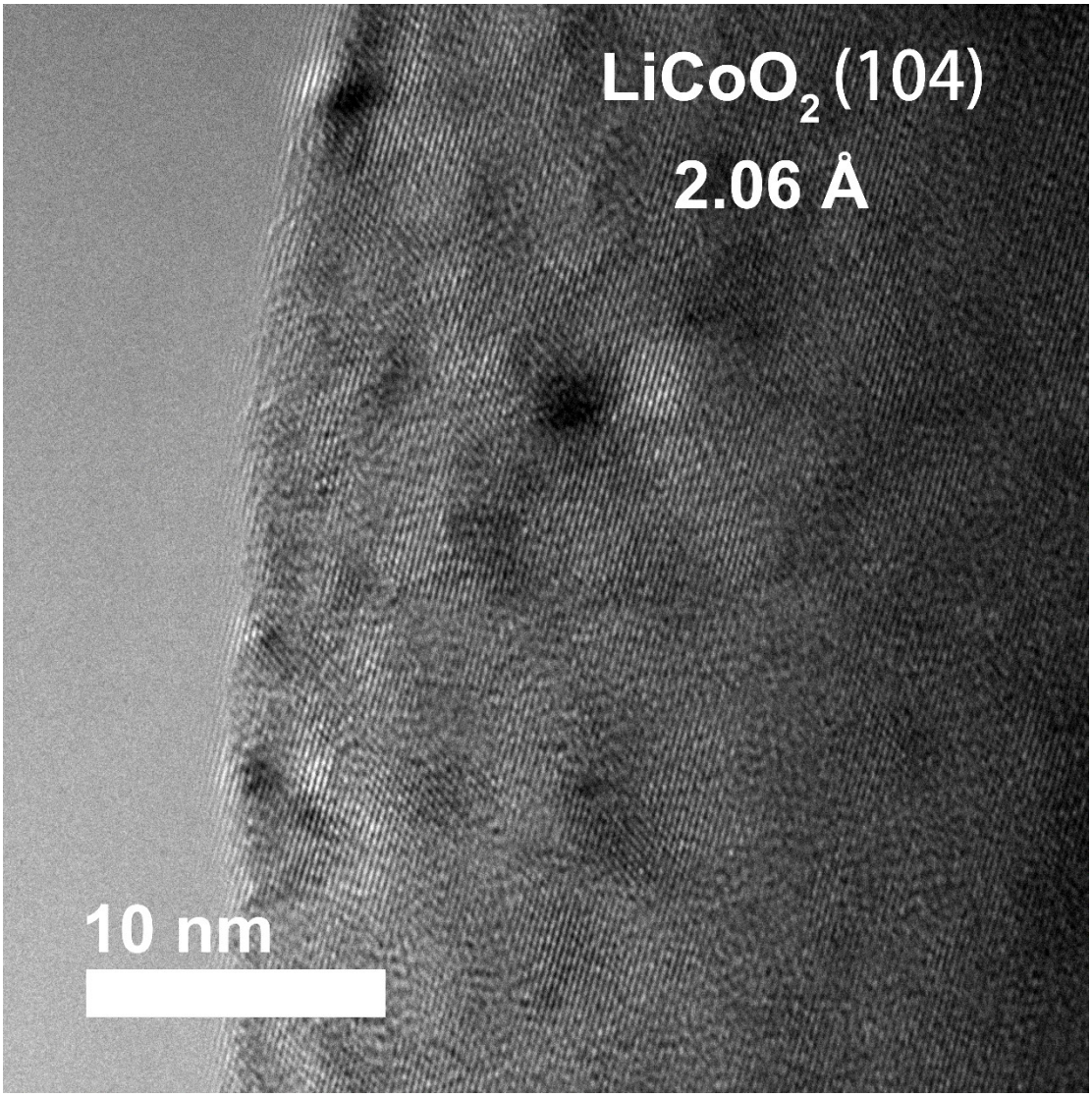

Fig. S12 HR-TEM image of the bare LCO.

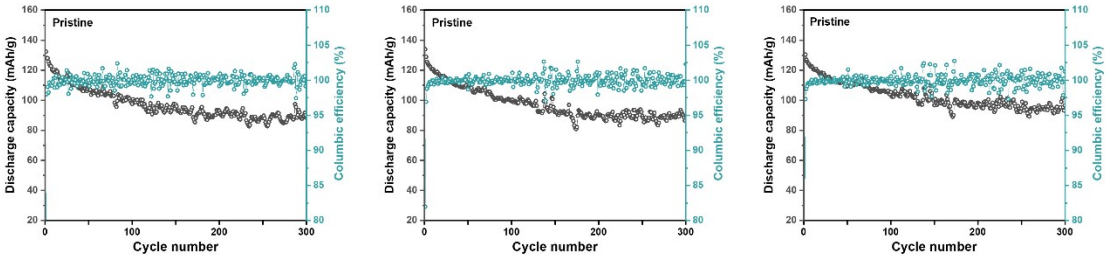

Fig. S13 Cycling performance of typical three solid-state batteries with the pristine LPSC electrolyte and LCO cathode at 0.5 C rate. The average capacity after 300 cycles is 91.5 mAh/g.

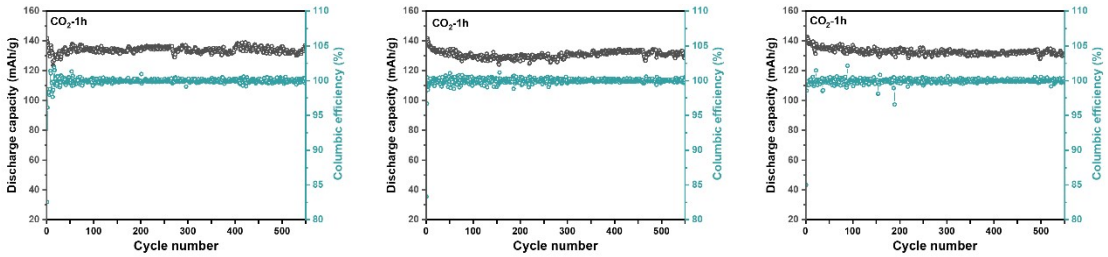

Fig. S14 Cycling performance of typical three solid-state batteries with the CO_2-1h LPSC electrolyte and LCO cathode at 0.5 C rate. The average capacity after 550 cycles is 132.1 mAh/g.

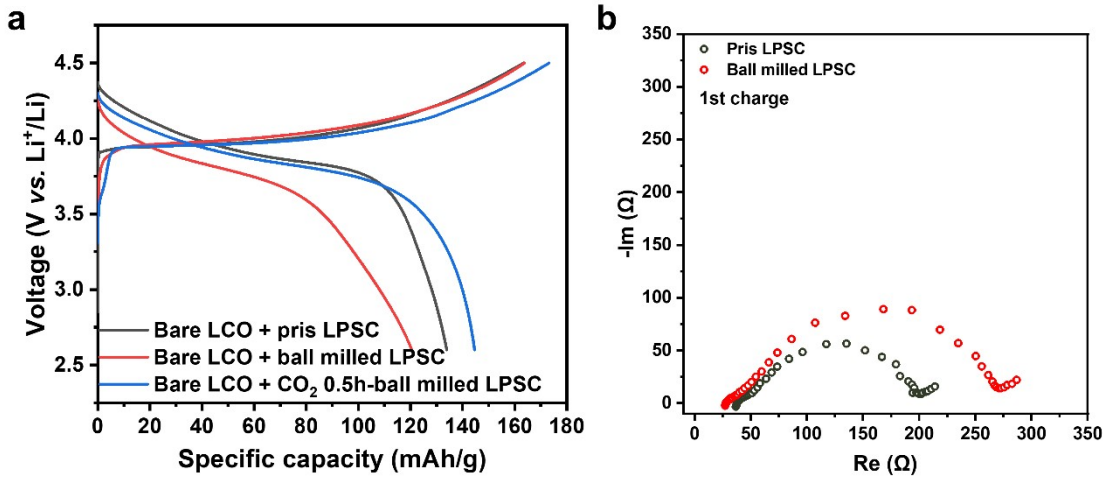

Fig. S15 Electrochemical performance for the ball-milled LPSC. (a) The initial charge-discharge voltage between 2.6 - 4.5 V *vs.* Li^+/Li at 0.5 C rate. (b) Impedance spectra after 1st discharge. After ball milling, the side reaction is exaggerated by the enhanced contact between cathode particles and LPSC particles leading to larger polarization and impedance, which is significantly hindered by Li_2CO_3 coating.

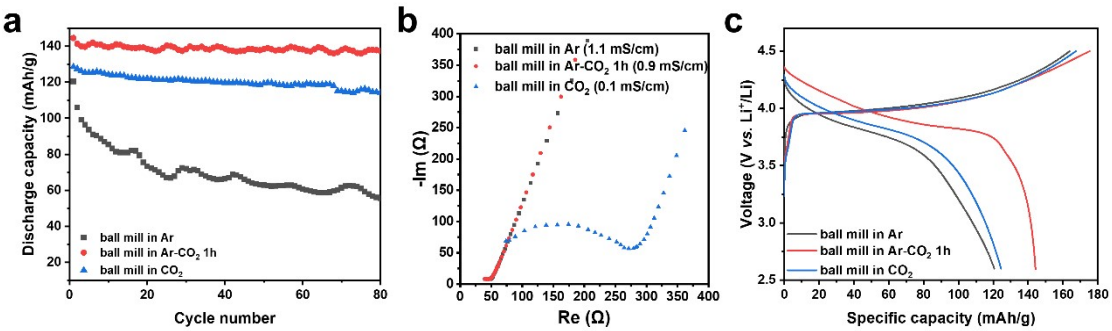

Fig S16 (a) Cycling performance of ASSBs at 0.5 C with various ball-milled LPSC. (b) Ionic conductivity measurement of LPSC after different ball milling process. (c) The initial voltage profiles of ASSBs at 0.5 C with ball-milled LPSC.

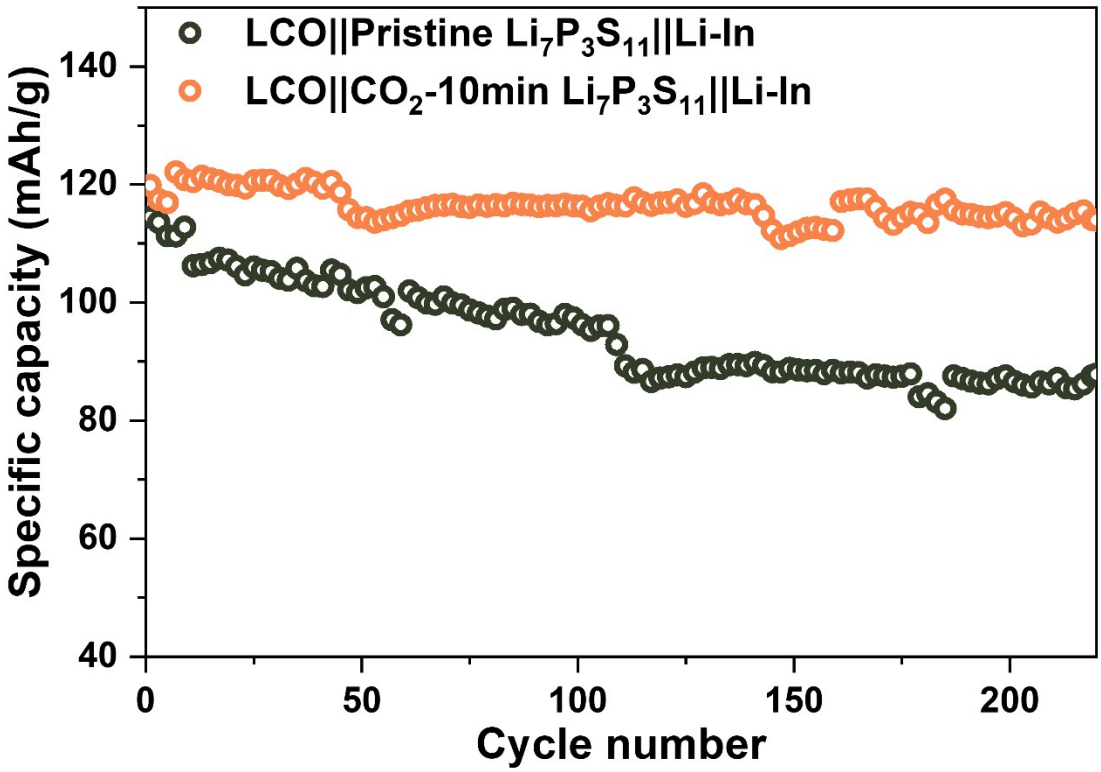

Fig. S17 Cycling performance of LCO half-cell using $Li_7P_3S_{11}$ as electrolyte.

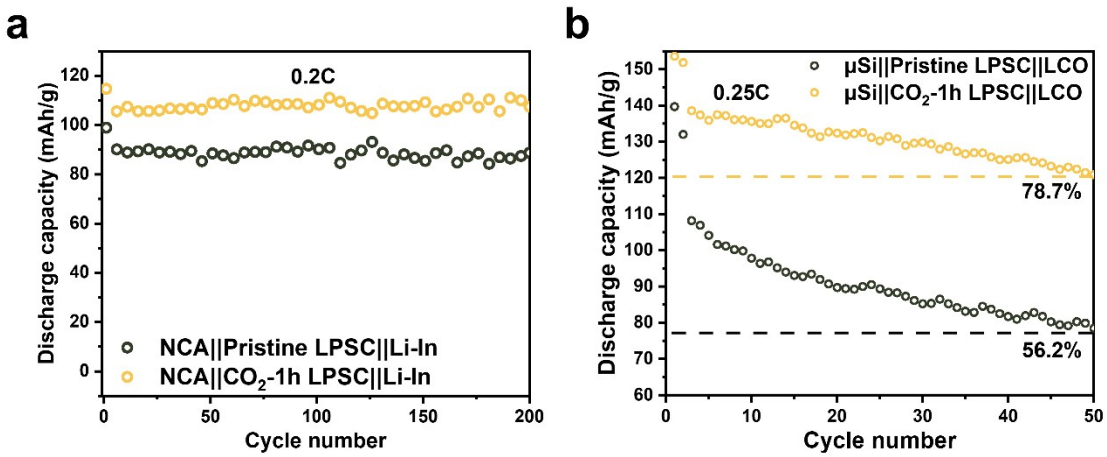

Fig. S18 Electrochemical performance of ASSBs. (a) Cycling performance of Li-In||SE||NCA half-cell. (b) Cycling performance of Si||SE||LCO full cell.

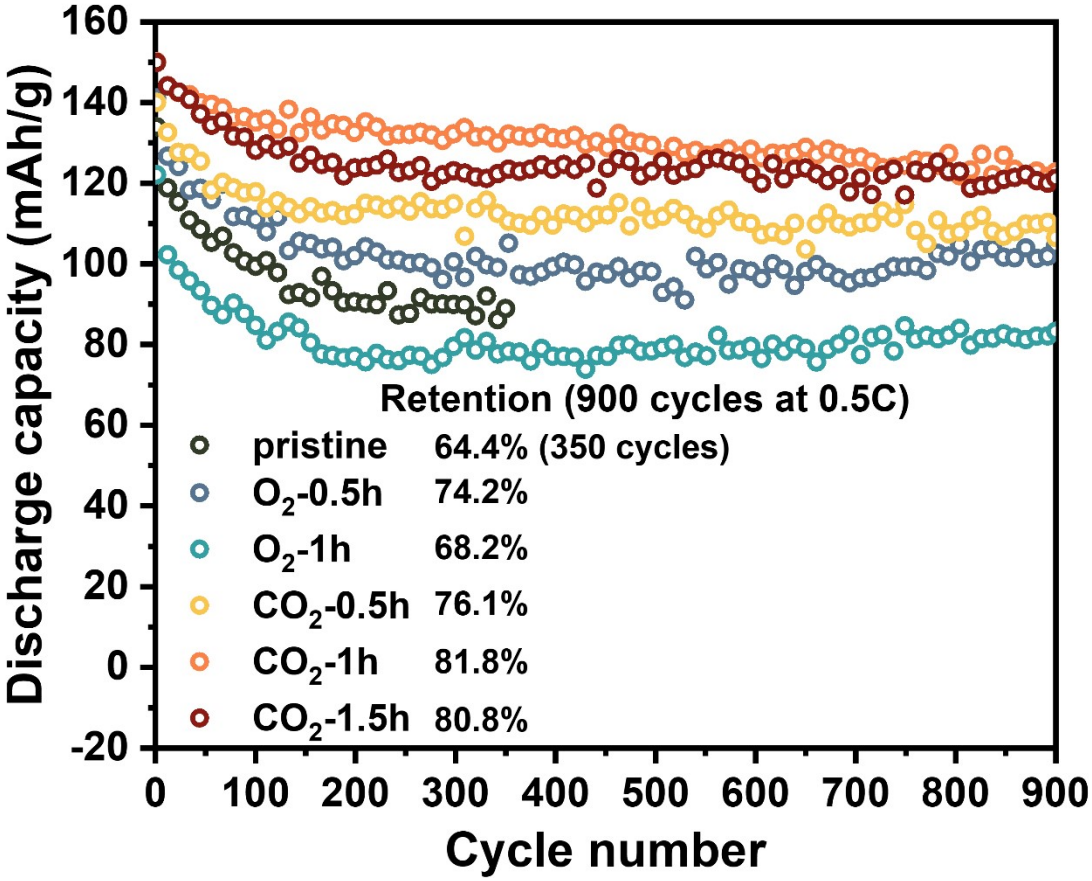

Fig. S19 Cycling performance of LCO half cells using pristine LPSC as electrolyte layer and the modified LPSC samples were only used in cathode composites. CO_2-treated samples show better cycling performance.

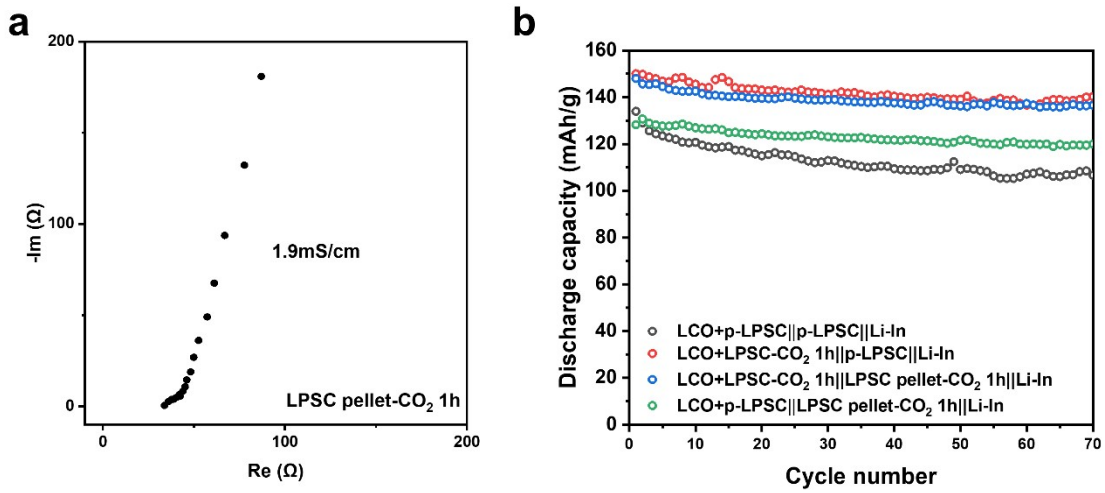

Fig.S20 (a) Ionic conductivity measurement of LPSC pellet after CO_2 treatment. (b) Cycling performance of ASSBs at 0.5 C with different combinations. Only applying the modified LPSC pellet (LCO+p-LPSC||LPSC pellet-CO_2 1h) exhibits improved electrochemical performance than the untreated one but is inferior to those using modified LPSC in the cathode composite since majority of interfacial reactions happen in the cathode composite.

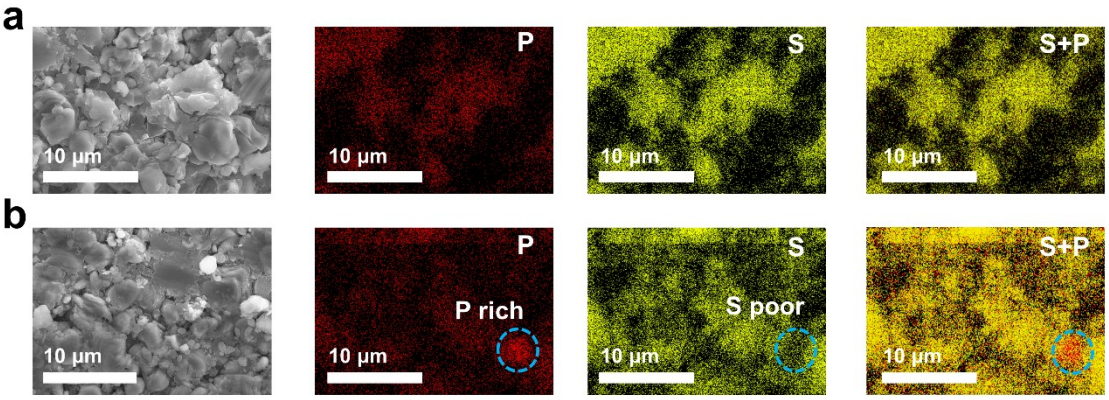

Fig. S21 EDS mapping of the CO_2-1h LPSC/LCO composite (a) and the pristine LPSC/LCO composite (b) after 100 cycles. P, and S are almost evenly distributed in the CO_2-1h LPSC/LCO composite after 100 cycles while elemental separation is visible in the LPSC/LCO composite without CO_2 treatment, indicating that severe side reaction occurs in the latter which is hindered by the Li_2CO_3 coating in the former.

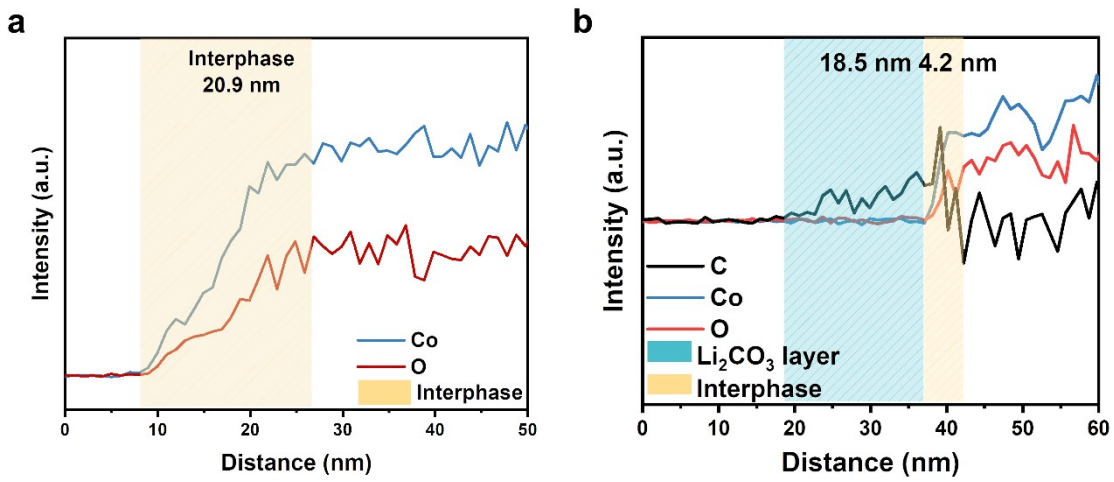

Fig. S22 EELS line profiles of Co/O/C for the $LiCoO_2$ with the pristine LPSC (a) and the $LiCoO_2$ with the CO_2-1h LPSC (b) after 100 cycles. The CEI thickness is about 20.9 nm and 4.2 nm with the pristine LPSC and CO_2-1h LPSC, respectively.

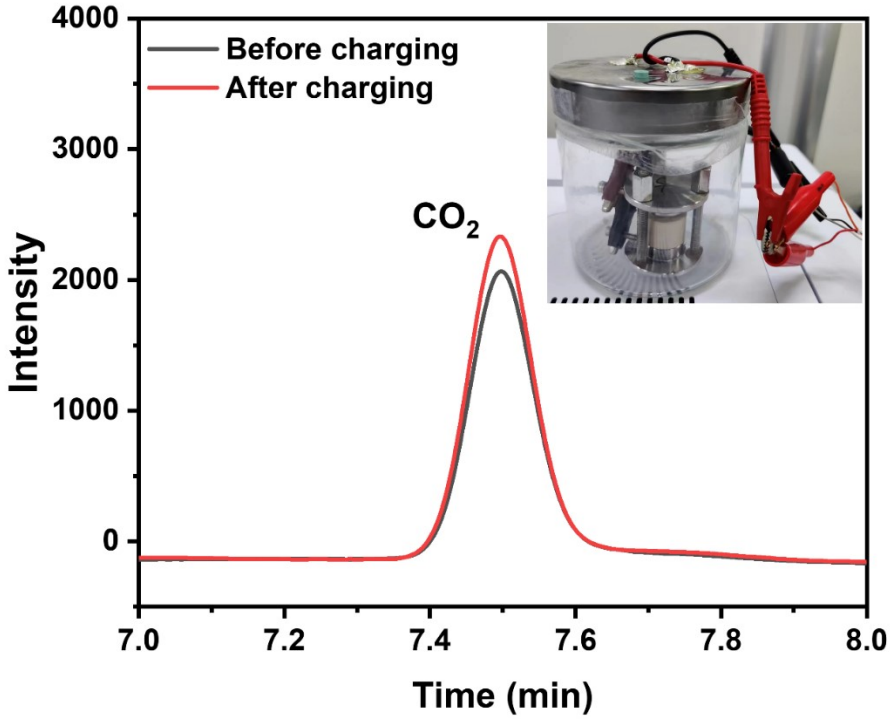

Fig. S23 CO_2 content evolution after charging measured by GC. The CO_2 before the charging is originated from the atmosphere in the Ar-filled glovebox.

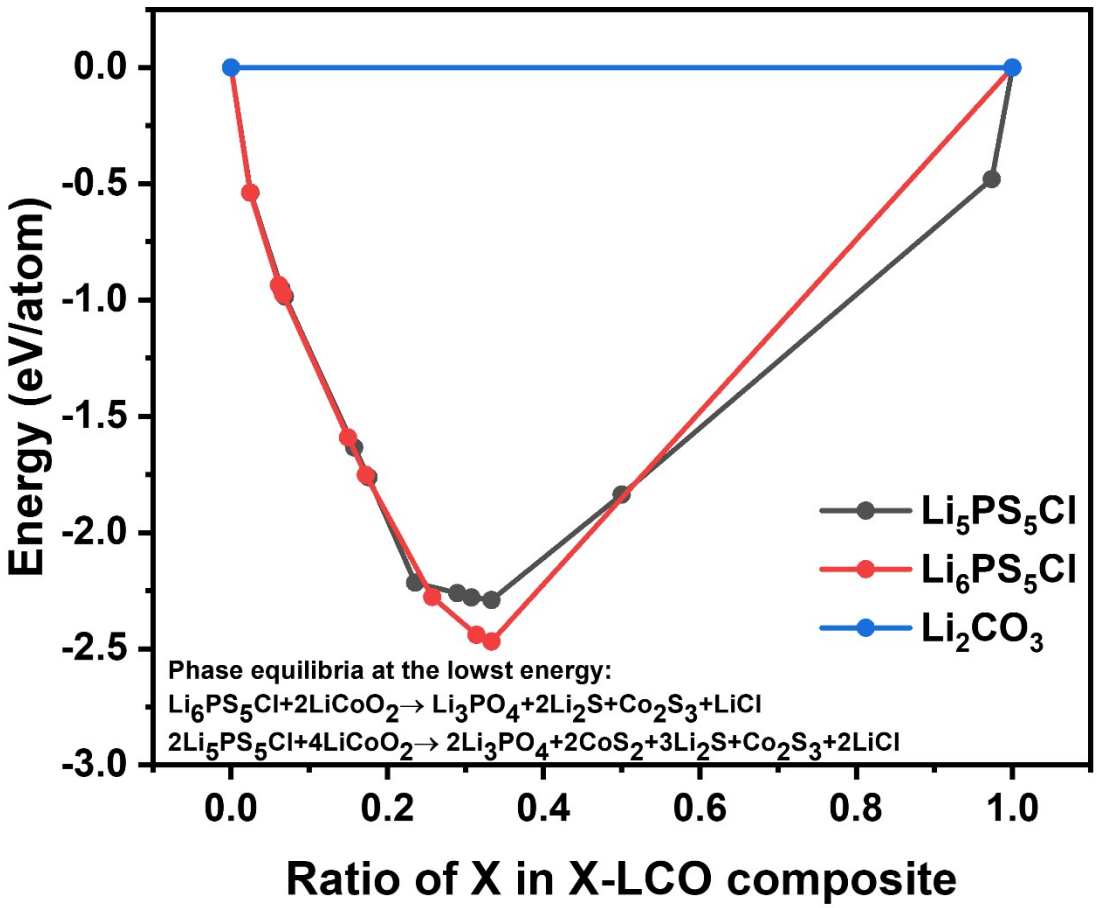

Fig. S24 Calculated mutual reaction energy between SSE and $LiCoO_2$. Li_5PS_5Cl and Li_6PS_5Cl show similar mutual reaction energy with $LiCoO_2$ albeit the Li_5PS_5Cl has a slightly higher mutual reaction energy than Li_6PS_5Cl. Considering the nonreactivity between Li_2CO_3 and $LiCoO_2$, we believe that the dominant contribution to the interfacial stability is from Li_2CO_3 rather than Li_5PS_5Cl.

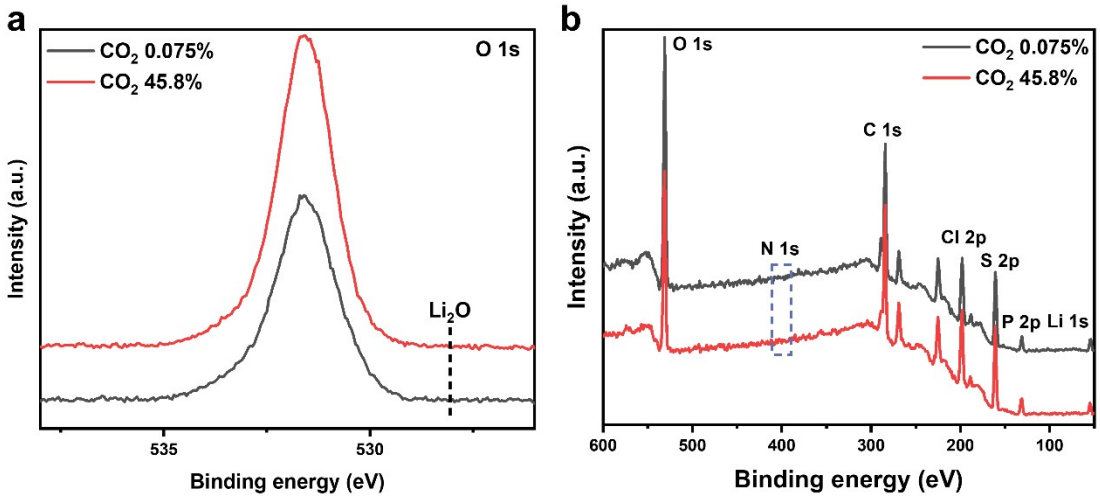

Fig. S25 The XPS O 1s spectra (a) and the survey spectra (b) of the pristine LPSC electrolytes after exposure to the CO_2 atmosphere with different concentration for 30 mins.

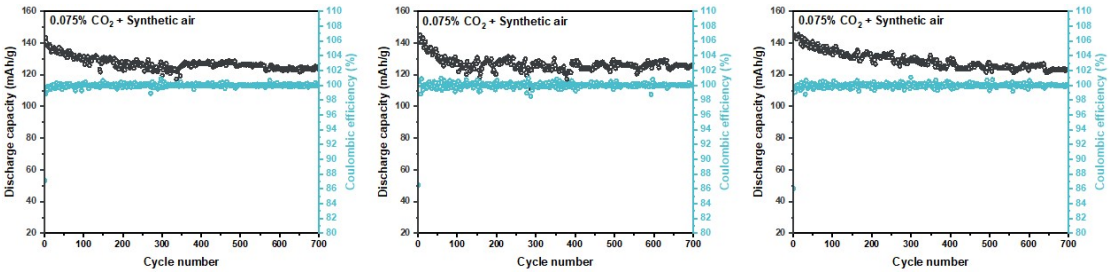

Fig. S26 Cycling performance of typical three solid-state batteries assembled in the dry air containing 0.075% CO_2 at 0.5 C rate. The average capacity after 700 cycles is 124.0 mAh/g.

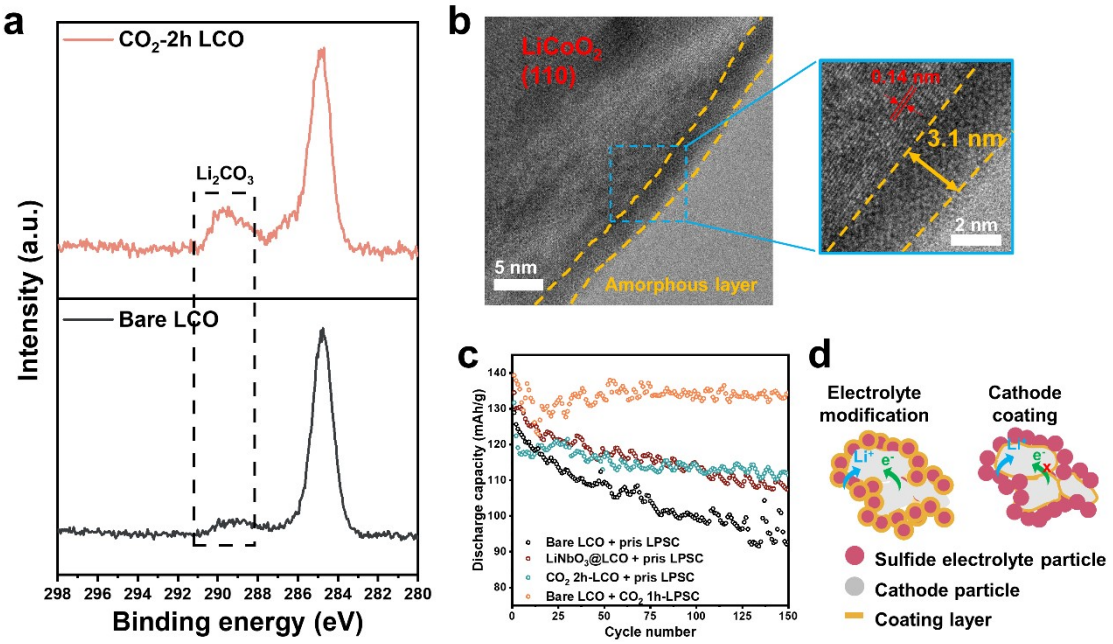

Fig. S27 Comparison of coating $LiCoO_2$ with Li_2CO_3. (a) XPS spectra of $LiCoO_2$. (b) HR-TEM image of $LiCoO_2$ surface after annealing in CO_2. (c) Cycling performance comparison between cathode coating and electrolyte modification strategies. (d) Illustration of Li^+/e^- transportation in case of cathode coating and electrolyte modification.

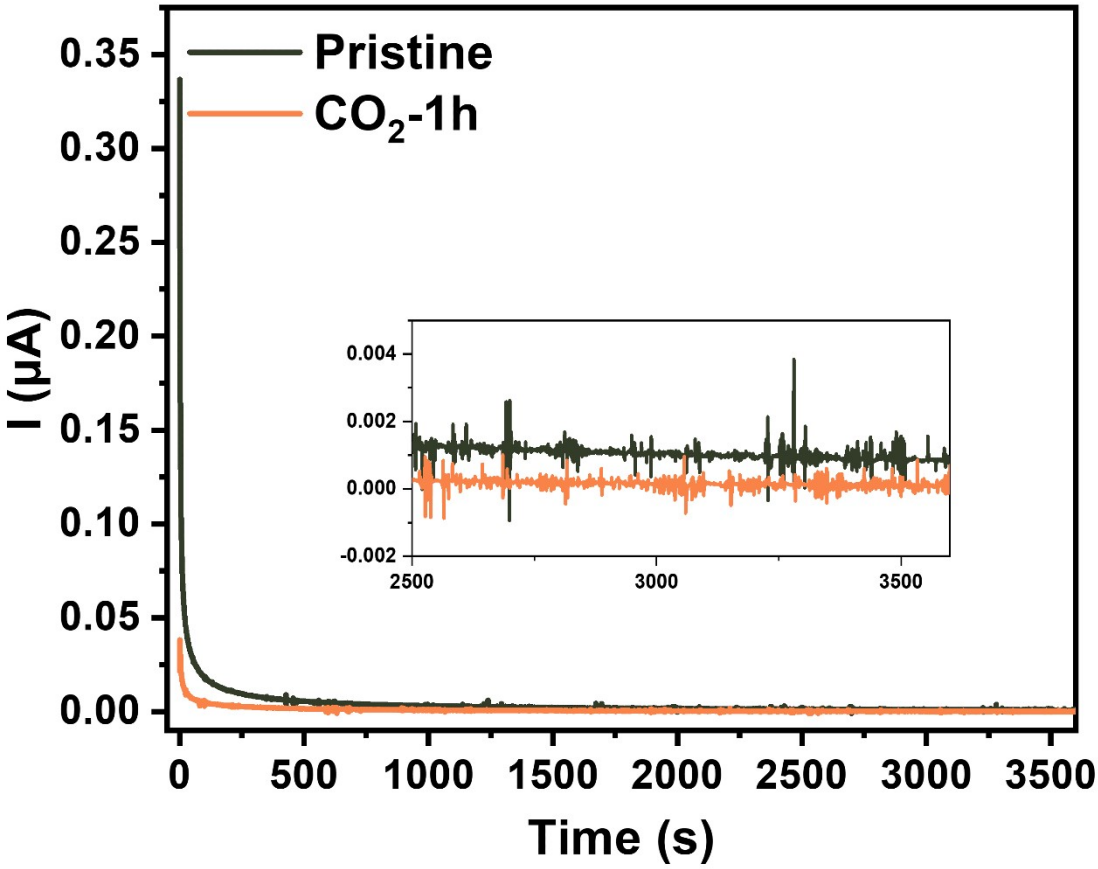

Fig. S28 Comparison of electronic conductivity of the pristine LPSC and CO_2-1h LPSC samples measured by DC polarization. The corresponding electronic conductivity of the pristine LPSC sample is 1.53×10^{-11} S/cm and CO_2-1h LPSC sample is 2.1×10^{-11} S/cm.

Table S1. Energy of species in Equation 1 calculated by DFT. Thus, the activation energy of Equation 1 was calculated to be -142.33 kJ/mol

Species	Energy
2 Li_6PS_5Cl	-107.099 eV
2 CO_2	-45.906 eV
Li_2CO_3	-39.398 eV
CO	-14.776 eV
Li_5PS_5Cl	-100.278 eV

Table S2. Cycling performance comparison of this work with other sulfide-based ASSBs using $LiCoO_2$ as cathode reported in recent literature which were assembled in Ar-filled glovebox.

No.	Voltage / V *vs.* Li^+/Li	Current density / C rate	Cycle number	Capacity / mAh g^{-1}	Cycle retention	Ref.
1	4.5	0.2	100	136.9	95%	5
2	4.2	0.1	100	132.1	93%	6
3	4.2	1	100	92.6	80%	7
4	4.3	0.2	50	133.2	94%	8
5	4.28	0.5	200	108	88%	9
6	4.3	0.5	140	99.7	84%	10
7	4.4	0.1	200	106.2	81.9%	11
8	4.5	0.1	100	128.9	78.1%	12
9	4.2	0.1	100	95	75%	13
10	4.2	1	150	91.7	89%	14
11	4.2	0.2	200	131.2	82%	15
12	4.2	0.1	200	90.4	69%	16
13	4.2	0.1	160	104.5	83%	17
14	4.2	0.3	250	89	86%	18
15	4.2	0.5	200	81.5	85%	19
16	**4.5**	**0.5**	**2100**	**126.9**	**89.4%**	**This work**

Reference

1 G. Kresse and J. Furthmüller, *Phys. Rev. B*, 1996, **54**, 11169.

2 J. P. Perdew, K. Burke and M. Ernzerhof, *Phys. Rev. lett.*, 1996, **77**, 3865.

3 G. L. Hart and R. W. Forcade, *Phys. Rev. B*, 2008, **77**, 224115.

4 S. Zhang, G. Yang, S. Liu, X. Li, X. Wang, Z. Wang and L. Chen, *Nano Energy*, 2020, **70**, 104486.

5 L. Wang, X. Sun, J. Ma, B. Chen, C. Li, J. Li, L. Chang, X. Yu, T. S. Chan and Z. Hu, *Adv. Energy Mater.*, 2021, **11**, 2100881.

6 Z. Sun, Y. Lai, N. Lv, Y. Hu, B. Li, S. Jing, L. Jiang, M. Jia, J. Li and S. Chen, *Adv. Mater. Interfaces*, 2021, **8**, 2100624.

7 G. Liu, W. Weng, Z. Zhang, L. Wu, J. Yang and X. Yao, *Nano Lett.*, 2020, **20**, 6660-6665.

8 S. H. Jung, K. Oh, Y. J. Nam, D. Y. Oh, P. Brüner, K. Kang and Y. S. Jung, *Chem. Mater.*, 2018, **30**, 8190-8200.

9 Z. Li, Z. Wang, Y. Miao, Y. Ma, H. Zhang, X. Shi, D. Song, L. Zhang and L. Zhu, *J. Power Sources*, 2022, **541**, 231703.

10 L. Zhou, T.-T. Zuo, C. Y. Kwok, S. Y. Kim, A. Assoud, Q. Zhang, J. Janek and L. F. Nazar, *Nat. Energy*, 2022, 1-11.

11 N. Zhang, F. Ding, S. Yu, K. Zhu, H. Li, W. Zhang, X. Liu and Q. Xu, *ACS Appl. Mater. Inter.*, 2019, **11**, 27897-27905.

12 P. Lu, L. Liu, S. Wang, J. Xu, J. Peng, W. Yan, Q. Wang, H. Li, L. Chen and F. Wu, *Adv. Mater.*, 2021, **33**, e2100921.

13 X. Li, J. Liang, J. Luo, M. Norouzi Banis, C. Wang, W. Li, S. Deng, C. Yu, F. Zhao, Y. Hu, T.-K. Sham, L. Zhang, S. Zhao, S. Lu, H. Huang, R. Li, K. R. Adair and X. Sun, *Energy Environ. Sci.*, 2019, **12**, 2665-2671.

14 S. Deng, M. Jiang, A. Rao, X. Lin, K. Doyle-Davis, J. Liang, C. Yu, R. Li, S. Zhao and L. Zhang, *Adv. Funct. Mater.*, 2022, 2200767.

15 D. Cao, Q. Li, X. Sun, Y. Wang, X. Zhao, E. Cakmak, W. Liang, A. Anderson, S. Ozcan and H. Zhu, *Adv. Mater.*, 2021, **33**, 2105505.

16 C. Wang, J. Liang, M. Jiang, X. Li, S. Mukherjee, K. Adair, M. Zheng, Y. Zhao, F. Zhao and S. Zhang, *Nano Energy*, 2020, **76**, 105015.

17 J. Liang, X. Li, S. Wang, K. R. Adair, W. Li, Y. Zhao, C. Wang, Y. Hu, L. Zhang and S. Zhao, *J. Am. Chem. Soc.*, 2020, **142**, 7012-7022.

18 Z. Sun, Y. Lai, N. Lv, Y. Hu, B. Li, L. Jiang, J. Wang, S. Yin, K. Li and F. Liu, *ACS Appl. Mater. Inter.*, 2021, **13**, 54924-54935.

19 J. Gao, X. Sun, C. Wang, Y. Zhang, L. Yang, D. Song, Y. Wu, Z. Yang, T. Ohsaka and F. Matsumotoc, *ChemElectroChem,* 2022 , **9**, e202200156.